PAPER REVIEW 2019.05.07

Impacts of Topography on Airflow and Precipitation in the Pyeongchang Area Seen from Multiple-Doppler Radar Observations

Tsai, C.-L., K. Kim, Y.-C. Liou, G. Lee, and C.-K. Yu, 2018: Impacts of topography on airflow and precipitation in the Pyeongchang area seen from multiple-Doppler radar observations. Mon. Wea. Rev., 146, 3401–3424.

Impacts of Topography on Airflow and Precipitation in the Pyeongchang Area Seen from Multiple-Doppler Radar Observations

CHIA-LUN TSAI[a]

Department of Astronomy and Atmospheric Sciences, and Center for Atmospheric Remote Sensing (CARE), Kyungpook National University, Daegu, South Korea

KWONIL KIM

Department of Astronomy and Atmospheric Sciences, Kyungpook National University, Daegu, South Korea

YU-CHIENG LIOU

Department of Atmospheric Sciences, National Central University, Jhongli, Taiwan

GYUWON LEE

Department of Astronomy and Atmospheric Sciences, and Center for Atmospheric Remote Sensing (CARE), Kyungpook National University, Daegu, South Korea

CHENG-KU YU

Department of Atmospheric Sciences, National Taiwan University, Taipei, Taiwan

(Manuscript received 29 December 2017, in final form 9 August 2018)

Outlines

- Introduction
- Data and methodology
  - Observational data
  - WISSDOM
- Overview of the studied case
  - LPS and precipitation
  - Environmental conditions
- Structural evolution of airflow and precipitation over topography
  - Stage I (0600 UTC 21 January 2013)
  - Stage II (1530, 1830 UTC 21 January 2013)
- Conclusions

Introduction

- Topography is one of the critical factors that determine the intensity and distribution of precipitation (Medina and Houze 2003; Rotunno and Ferretti 2003; Houze and Medina 2005; Rotunno and Houze 2007).

- Limited number of previous modeling studies have indicated that heavy rainfall and snowfall events occurred frequently near the TMR during winter (Lee and Park 1996; Lee and Kim 2008; Jung et al. 2012; Lee and Xue 2013).

- Pyeongchang hosted the Winter Olympics in 2018. Our work was completed prior to the Olympic Games as part of the effort to ensure adequate forecasts, such as high-quality wind and precipitation information, were available to ensure the safety of all participants.

Introduction

- Topographically enhanced precipitation usually occurs during the passage of preexisting weather disturbances, and the interactions of such weather systems with topography are complex because of temporally changing environmental conditions (Roe 2005; Smith 2006; Houze 2012).

- Medina et al. (2007) showed that enhanced precipitation could be produced by interactions between turbulence and orography as extratropical cyclones move over the Cascade Range in Oregon.

- The region of the TMR is usually influenced by a northeasterly airflow in winter, with stronger cross-barrier flow and stable environmental conditions (Lee and Kim 2008; Jung et al. 2012).

Introduction

- Lee and Kim (2008) utilized WRF model to investigate topographic effects on snowfall distribution near the TMR. Stronger northeasterly winds were lifted over the windward side, causing heavy snowfall on the northeastern slope of the TMR.

- Park and Lee (2009) used multiple-Doppler radar to retrieve the wind field over the southern Korean Peninsula. Limitations of Doppler radar should be considered, particularly beam blockage over complex mountainous areas in the Pyeongchang area.

- The objective of this study was to identify the mechanisms of wintertime precipitation over these topographic features during the passage of a low pressure system (LPS) through the southern Korean Peninsula.

Data: Information of South Korea

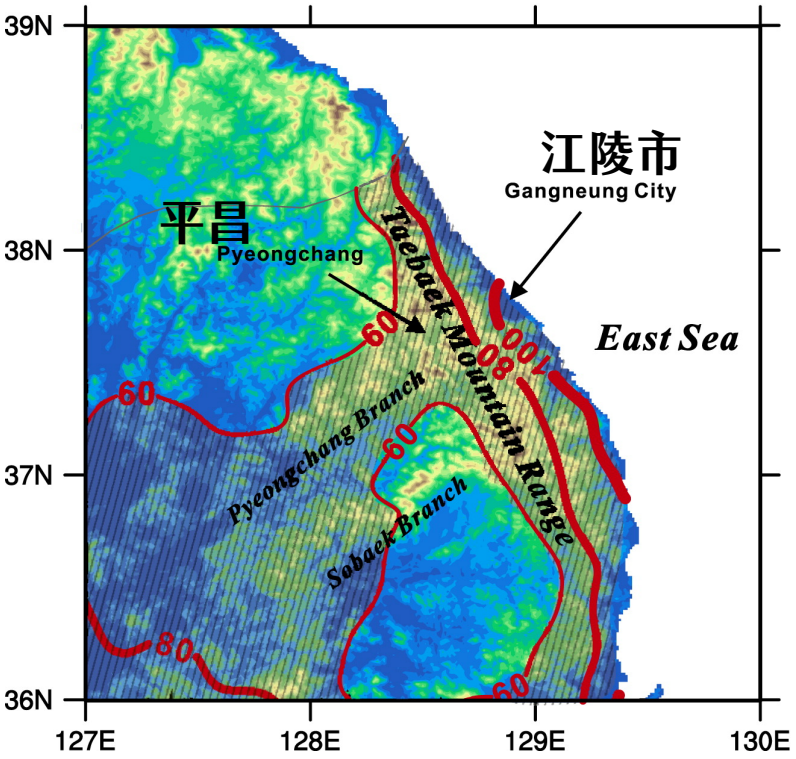

Fig 01

Shading: Topography

Contour:

Climatology of total precipitation in winter (mm) 2004 -2015 from AWS

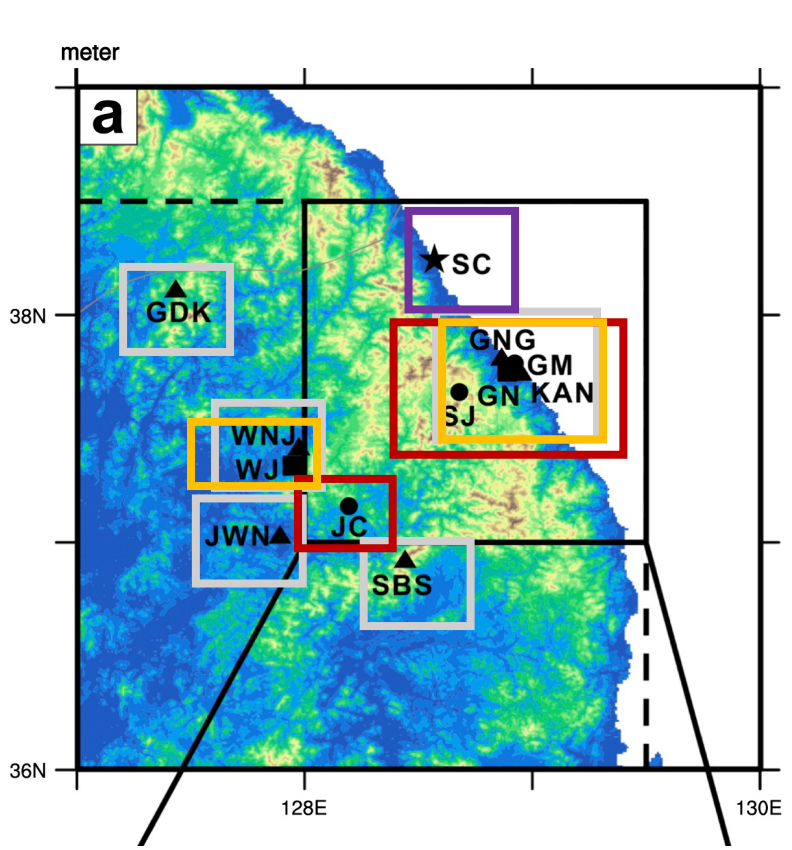

Fig 02

Shading: Topography

▲ Radar (every 10min)

KMA S-band: GDK, GNG

KAF C-band: JWN, WNJ, KAN

MOLIT dual-Pol S-band: SBS

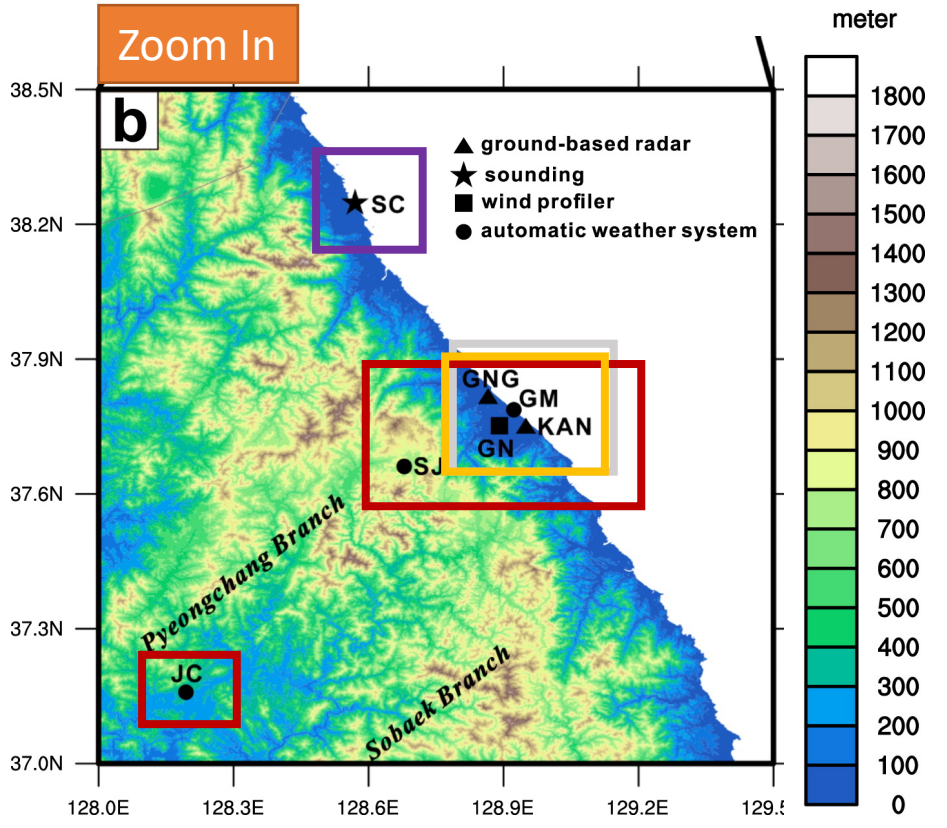

★ Sounding (every 12h): SC 束草市

■ wind profiler (every 10min, dz=70 m, Zmax=5 km): WJ (原州市) , GN (江陵市)

● AWS (automatic weather system, every 1 min): JC , SJ, GM

Data: Radar

- KHSR method: construct a dataset from the lowest available radar reflectivity to analyze the horizontal distribution of the precipitation. (Kyungpook National University hybrid surface rainfall; Kwon et al. 2015; Lyu et al. 2015; Kwon 2016).

- Fuzzy logic algorithm: eliminate non-meteorological radar echoes (Cho et al. 2006; Ye et al. 2015).

Parameters	GDK	GNG	WNJ	JWN	KAN	SBS
Longitude (°E)	127.43	128.86	127.96	127.89	128.94	128.44
Latitude (°N)	38.11	37.81	37.43	37.03	37.75	36.92
Radar height (m)	1064	99	120	117	27	1408
Wavelength (cm)	10.4	10.5	5.6	5.3	5.3	10.5
Beamwidth (°)	1	0.9	1	1	1	1
PRF (Hz)	599	535	1180	1200	1200	999
Nyquist velocity ($m\,s^{-1}$)	30.9	56.2	16.6	48.2	48.2	26.2
Max range (km)	250	280.25	89	125	125	149.12
Pulse width (μs)	1	1	1	0.8	0.8	1
Range resolution (m)	250	250	1000	1000	1000	125
Elevations (°)	0.0, 0.1, 0.2, 0.3, 0.6, 1.0, 1.7, 2.8, 4.6, 7.6, 12.3, 20	0.4, 0.6, 0.8, 1.1, 1.4, 1.8, 2.4, 3.0, 3.9, 4.9, 6.2, 7.9, 10, 12.7, 16, 20	1.6, 2.1, 2.8, 3.7, 4.9, 6.4, 8.3, 10.7, 13.7, 17.5, 22.2, 27.8, 34.4	1.8, 2.3, 2.9, 3.7, 4.6, 5.7, 7.1, 8.8, 10.8, 13.3, 16.3, 19.9, 24.2, 29.1, 34.6, 80	0.5, 0.9, 1.3, 1.8, 2.5, 3.3, 4.5, 5.9, 7.7, 10.1, 13.2, 17.1, 22, 28, 80	−0.5, 0.0, 0.3, 0.7, 1.0, 1.3

What is WISSDOM?

- WInd Synthesis System using DOppler Measurements is a variational-based multiple Doppler three-dimensional wind synthesis method (Liou and Chang 2009; Liou et al. 2012).

- Primary advantages:
  - Winds along the radar baseline can still be well recovered.
  - Resulting 3D flow fields satisfy a simplified vertical vorticity equation.
  - Any number of radars can be easily merged.
  - Wind field can be synthesized over complex terrain.
  - Background wind field can be attained from a combination of the sounding observations, reanalysis data, and/or output from the mesoscale model

WISSDOM: minimize 5 cost functions

$$J = \sum_{M=1}^{5} J_M \ [1]$$

i: radars(RCKT, RCCG, …)
t: time(2 observations)

P_{xyz}^{i}: $location\ of\ the\ ith-radar$
W_T: $Terminal\ veclocity\ from\ Z_H$ u_t, v_t, w_t: $desired\ wind\ field$

1- revised wind field → observation

$$r_i = \sqrt{(x-P_x^i)^2 + (y-P_y^i)^2 + (z-P_z^i)^2} \ [4]$$

$$J_1 = \sum_{t=1}^{2}\sum_{xyz}\sum_{i=1}^{5} \alpha_1 (T_{1,i,t})^2 \ [2] \qquad T_{1,i,t} = (V_r)_{i,t} - u_t \frac{(x-P_x^i)}{r_i} - v_t \frac{(y-P_y^i)}{r_i} - (w_t + W_T)\frac{(z-P_z^i)}{r_i} \ [3]$$

2- patch: use background field

$$J_2 = \sum_{t=1}^{2}\sum_{xyz} \alpha_2 (\vec{V}_t - \vec{V}_{B,t})^2 \ [5]$$

3- satisfy anelastic continuity equation

$$J_3 = \sum_{t=1}^{2}\sum_{xyz} \alpha_3 \left[\frac{\partial(\rho_{air} u_t)}{\partial x} + \frac{\partial(\rho_{air} v_t)}{\partial y} + \frac{\partial(\rho_{air} w_t)}{\partial z}\right]^2 \ [6]$$

4- satisfy simplified vertical vorticity eq.

$$J_4 = \sum_{xyz} \alpha_4 \left\{\frac{\partial \zeta}{\partial t} + [\overline{TA + TS + TT}]\right\}^2 \ [7]$$

$$\zeta \equiv \frac{\partial v}{\partial x} - \frac{\partial u}{\partial y} \ [8]$$

$$TA = u\frac{\partial \zeta}{\partial x} + v\frac{\partial \zeta}{\partial y} + w\frac{\partial \zeta}{\partial z} \ [9]$$

$$TB = (\zeta + f)\left(\frac{\partial u}{\partial x} + \frac{\partial v}{\partial y}\right) \ [10]$$

$$TT = \frac{\partial w}{\partial x}\frac{\partial v}{\partial y} + \frac{\partial w}{\partial y}\frac{\partial u}{\partial z} \ [11]$$

5- smooth retrieval wind field and make sure the continuity along the grid

$$J_5 = \sum_{t=1}^{2}\sum_{xyz} \alpha_5 [\nabla^2 (u_t + v_t + w_t)]^2 \ [12]$$

$$\nabla^2 \equiv \frac{\partial^2}{\partial x^2} + \frac{\partial^2}{\partial y^2} + \frac{\partial^2}{\partial z^2} \ [13]$$

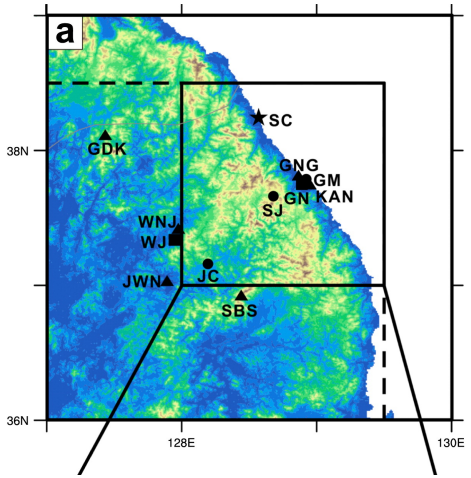

Main WISSDOM
1.5 degree x 1.5 degree
[150 km x 150 km]

dx= dy = 1 km
dz = 0.25 km
Z = 0 ~ 10 km MSL

Extended WISSDOM
2.5 degree x 2.5 degree
[250 km x 250 km]

Overview the case: LPS and precipitation

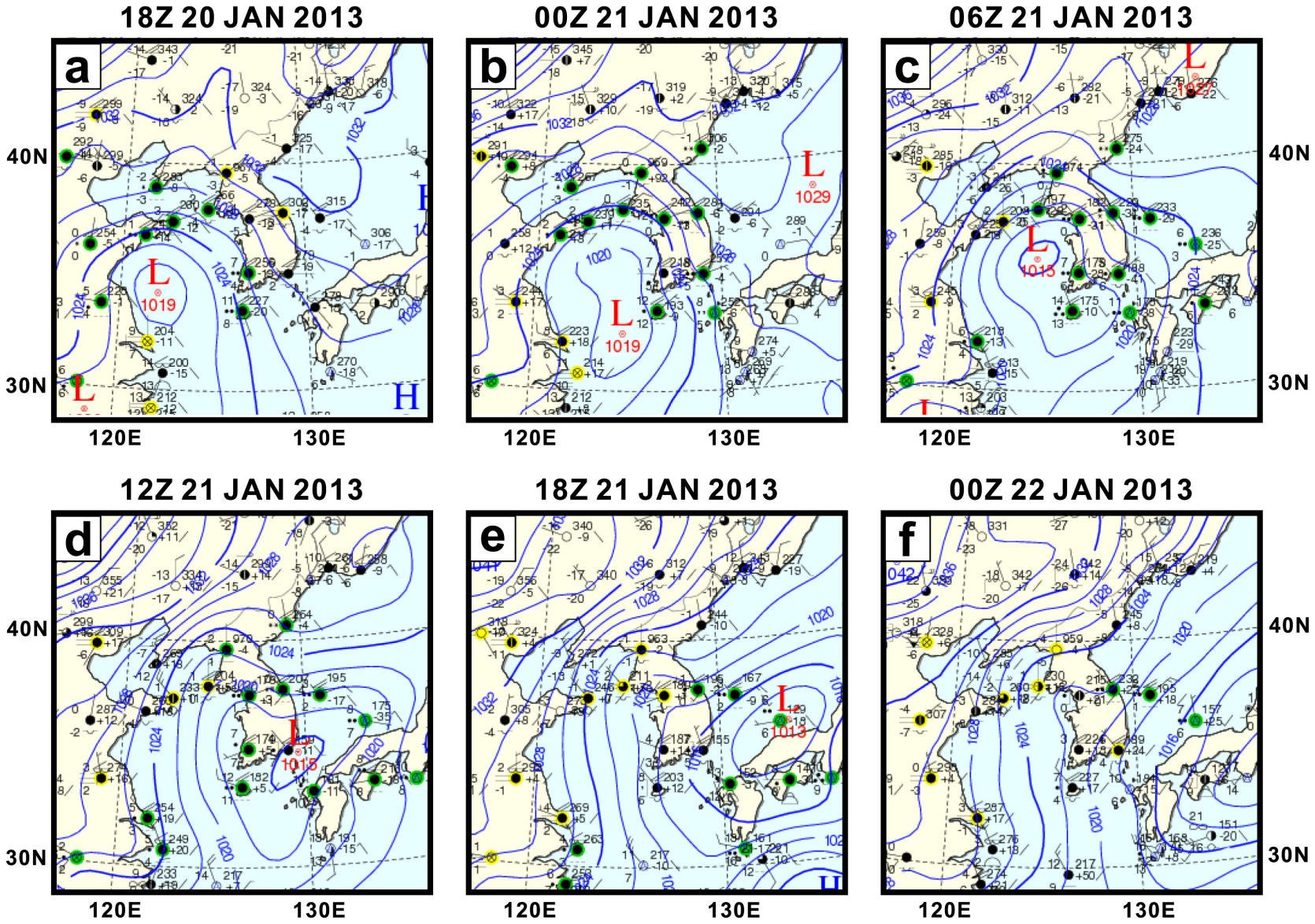

Fig 03

KMA surface analysis map obtained from 1800 UTC 20 Jan to 0000 UTC 22 Jan 2013 at 6-h intervals. Full wind barbs correspond to 5 m s^{-1}

Overview the case: LPS and precipitation

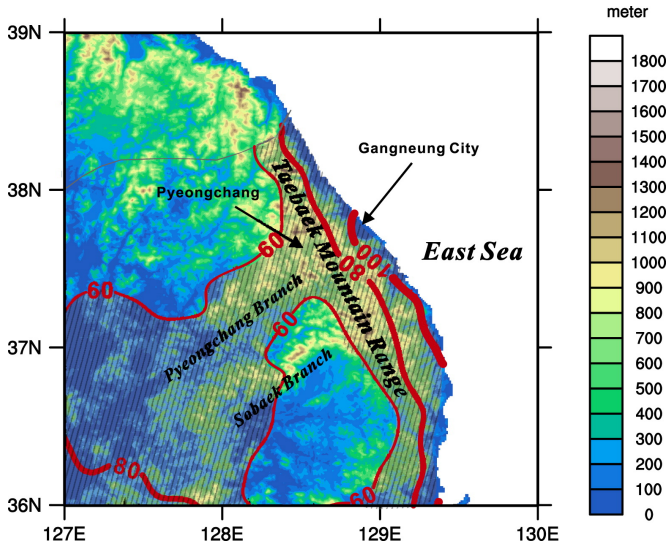

Fig 01
Shading: Topography

Red contour:
Climatology of total precipitation in winter (mm) 2004 -2015 from AWS

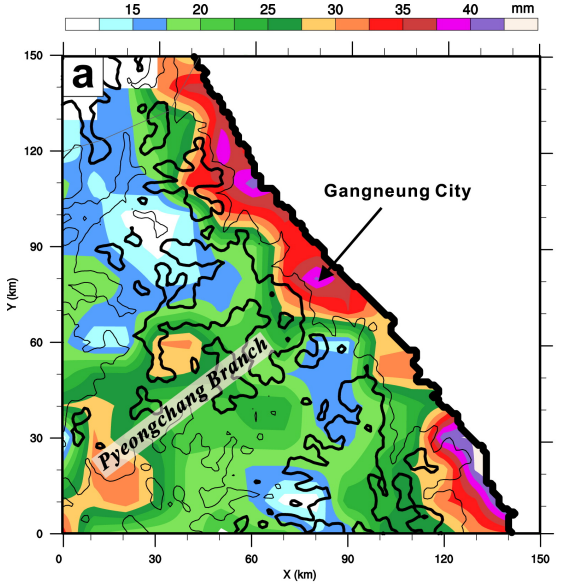

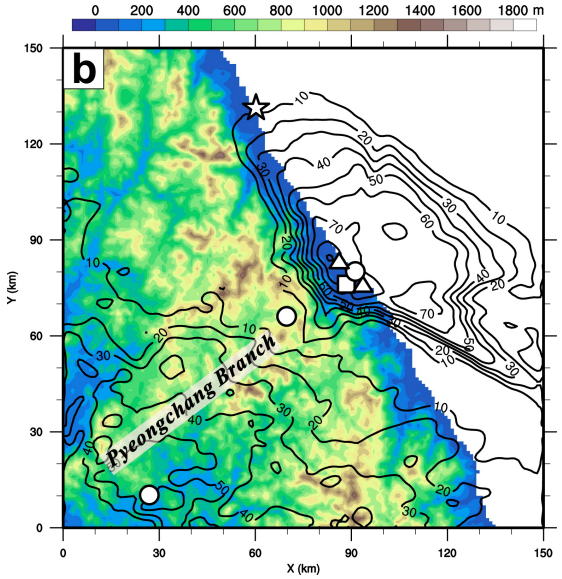

Fig 05 (a)
Shading: accumulated precipitation by the AWS in the WISSDOM domain from 1/20 20 UTC to 1/22 00 UTC

Black Contour: topography (400/800m)

Fig 05 (b)
Shading: topography

Black Contour: Frequency when the lowest available radar reflectivity >20 dB*Z* (%)

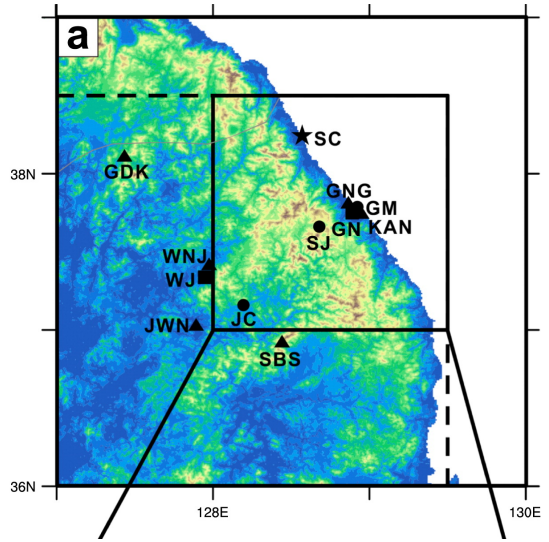

Fig 02
Shading: Topography
▲ Radar (every 10min)

KMA S-band: GDK, GNG

KAF C-band:
JWN, WNJ, KAN

MOLIT dual-Pol S-band:
SBS

Overview the case: LPS and precipitation

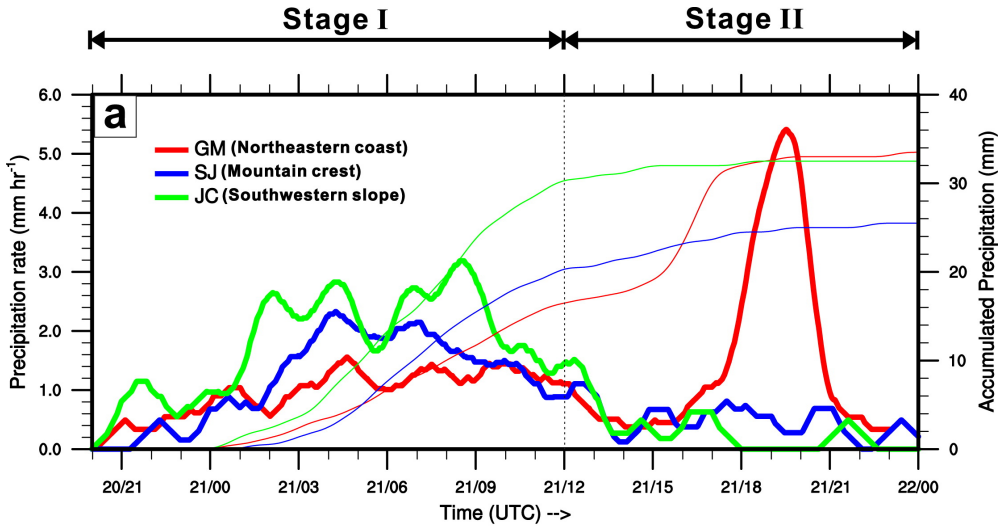

Fig 06 (a)

THICK lines: [mm h^{-1}]
Time series of precipitation rate

THIN lines: [mm]
Time series of accumulated precipitation

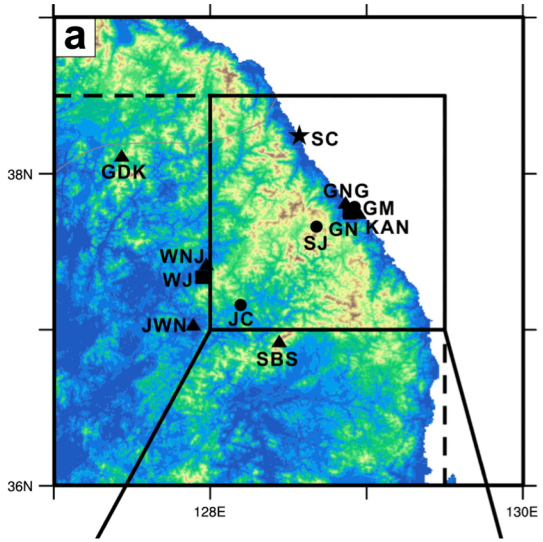

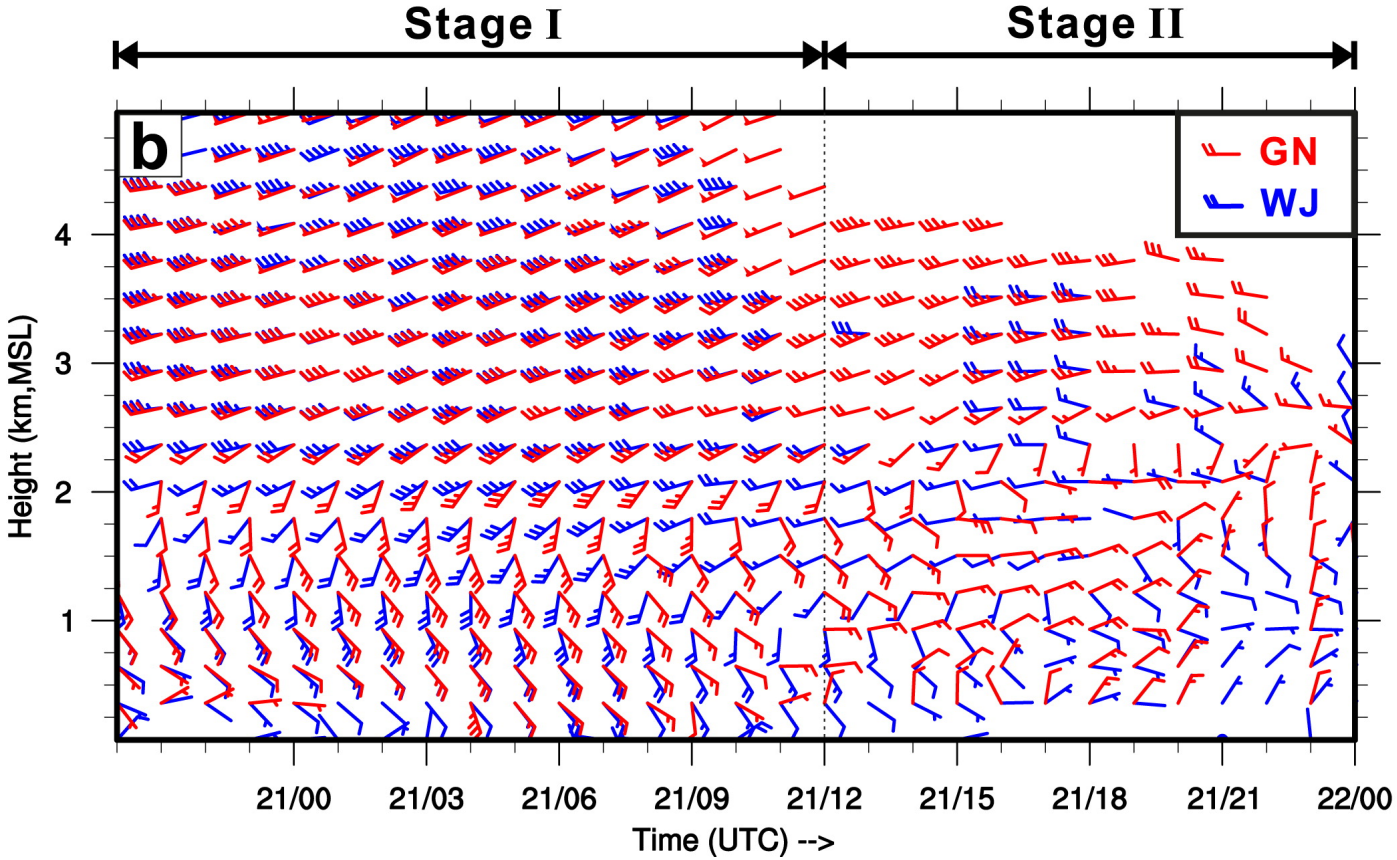

Fig 06 (b)

profiles of horizontal winds observed

WJ: mountain area / GN: coast area

Overview the case: Environmental conditions

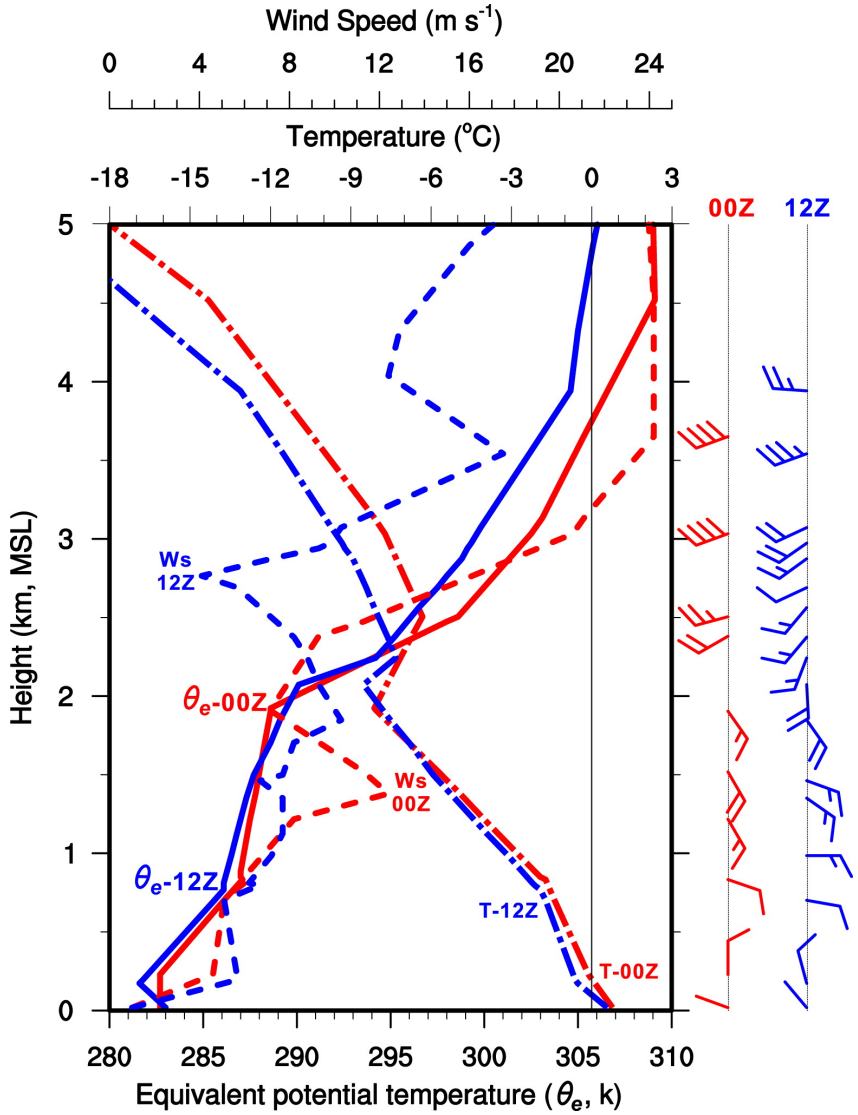

- Convectively stable environment
- Prevailing winds were clearly affected by topography below 500 m MSL
- Relative shallow influence from the LPS.
- F_r~ 0.79 to 0.86 (prevent airflow from climbing over topography)

Fig 07
Vertical profiles from SC sounding

dash–dotted: temperature
Solid: equivalent potential temperature
dash: wind speed Ws
Red: 1/21 00 UTC
Blue: 1/21 12UTC

$$F_r = \frac{U}{NH}$$

U: flow toward barrier
N: dry Brunt–Väisälä frequency
H: representative mountain height

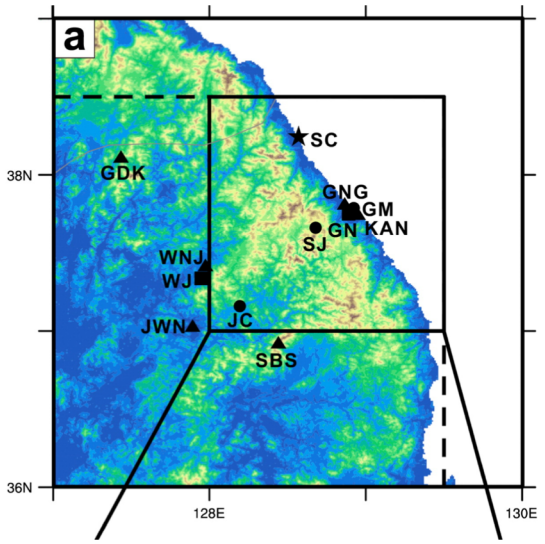

Structural evolution: Stage 1

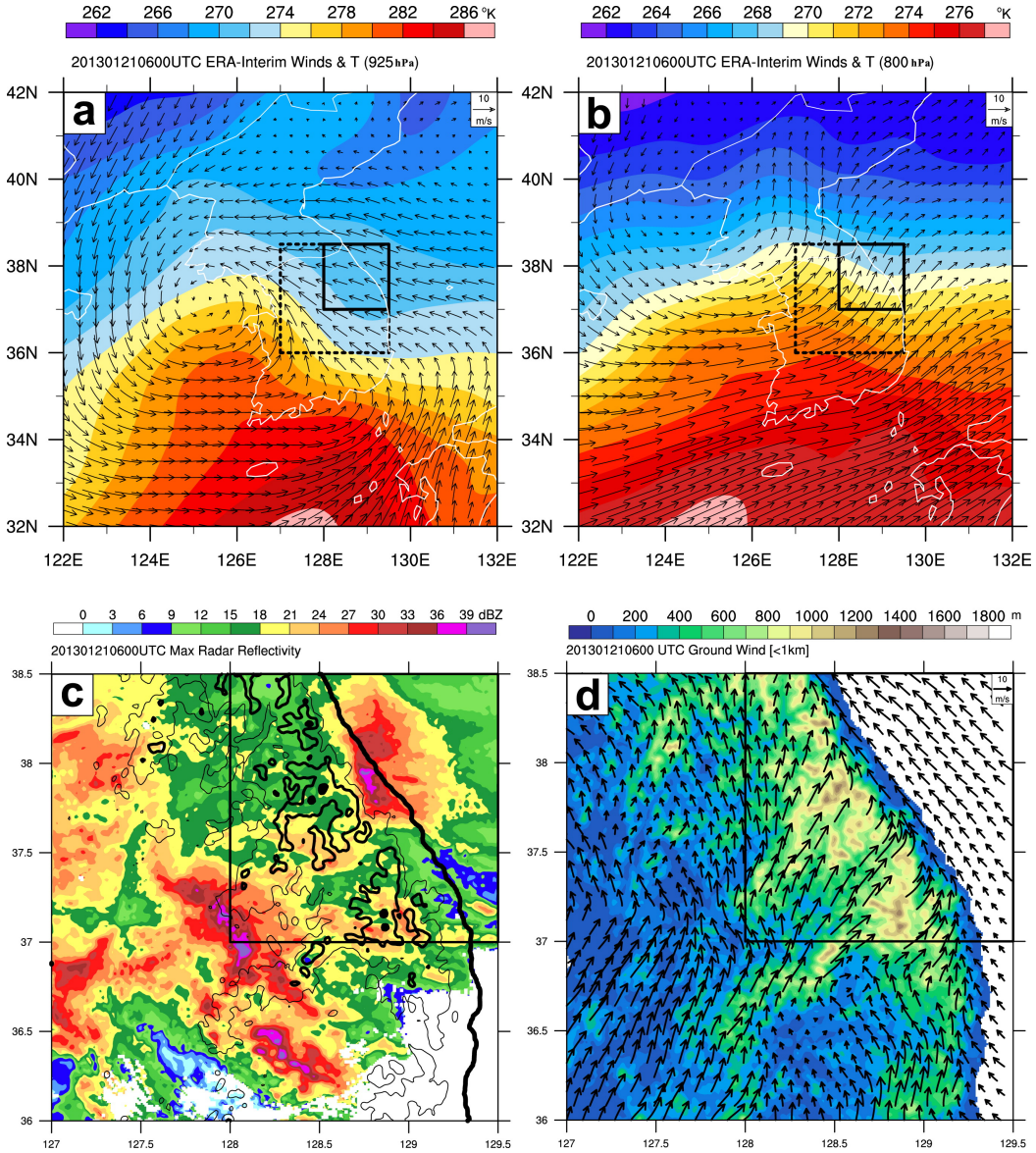

Fig 08

ERA-Interim 0.125 deg. 1/21 06UTC

Shading: temperature

(a) 925 hPa (b) 800 hPa

(c)

shading: max reflectivity

Black contour: topography (400/800/1200m)

(d)

Shading: topography

Wind: averaged ground-relative wind from WISSDOM (<1km MSL)

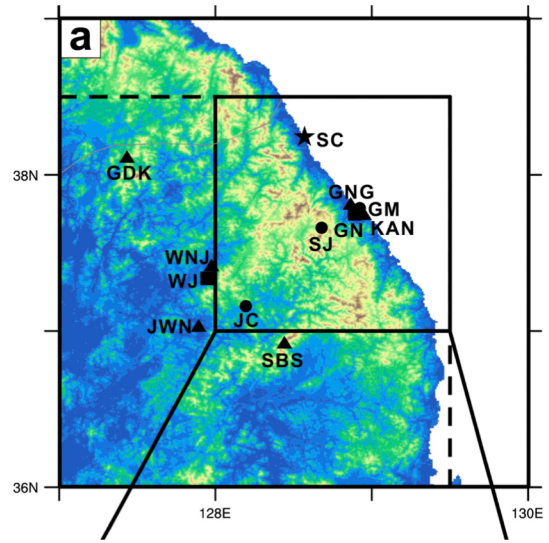

Structural evolution: Stage 1

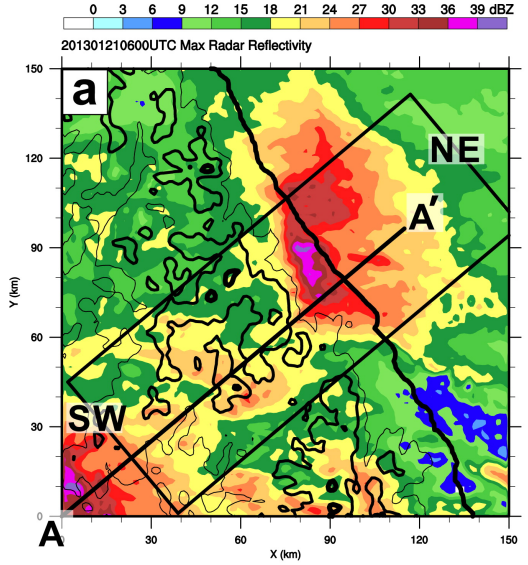

Fig 09

(a) shading: max reflectivity
Black contour: topography

(b) Shading: topography
Wind: averaged ground-relative wind from WISSDOM (<1km MSL)

(c) Shading: Horizontal divergence (10^{-4}/s)
Black contour: topography

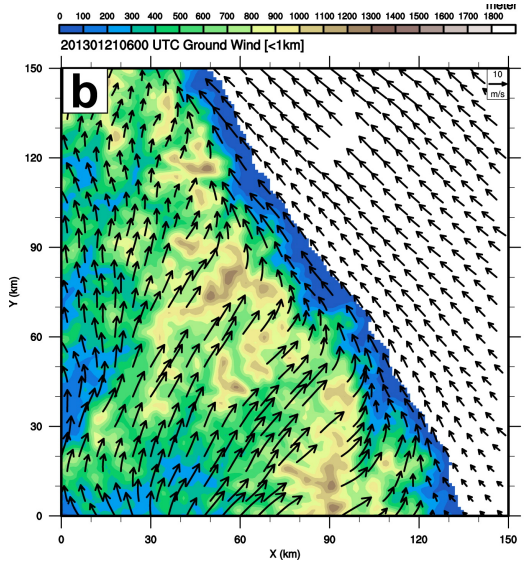

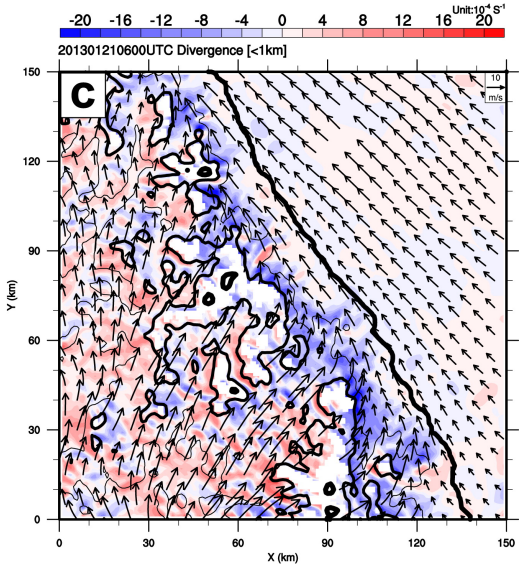

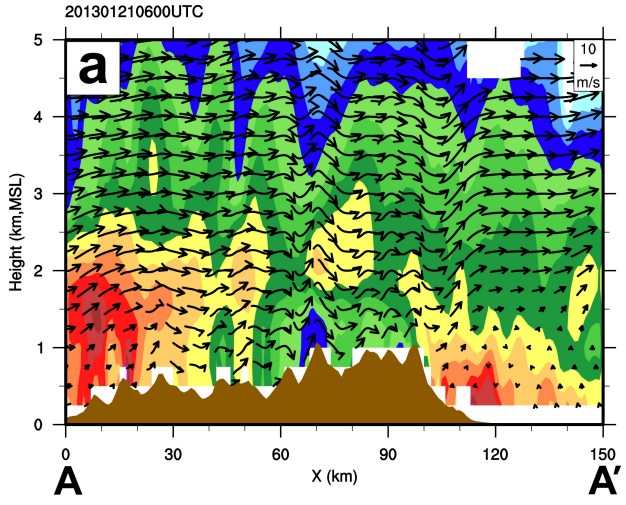

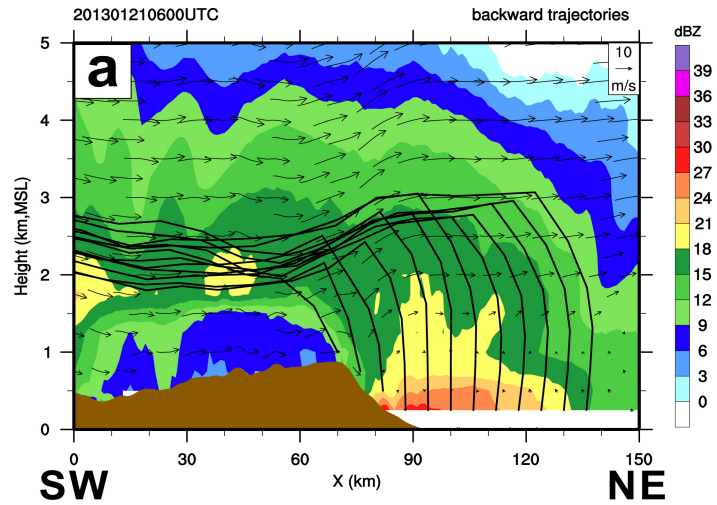

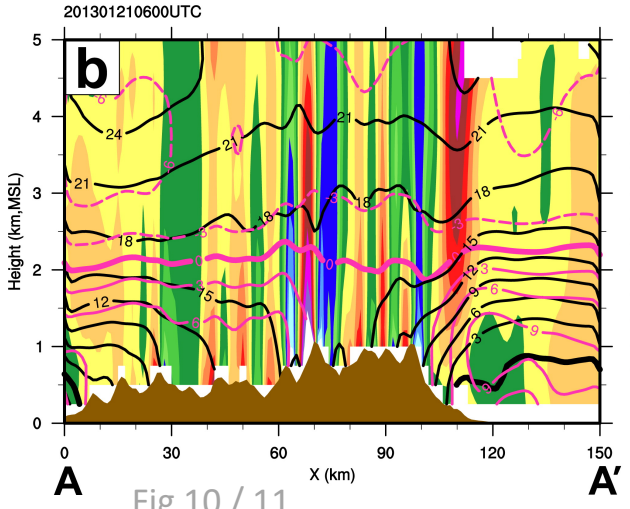

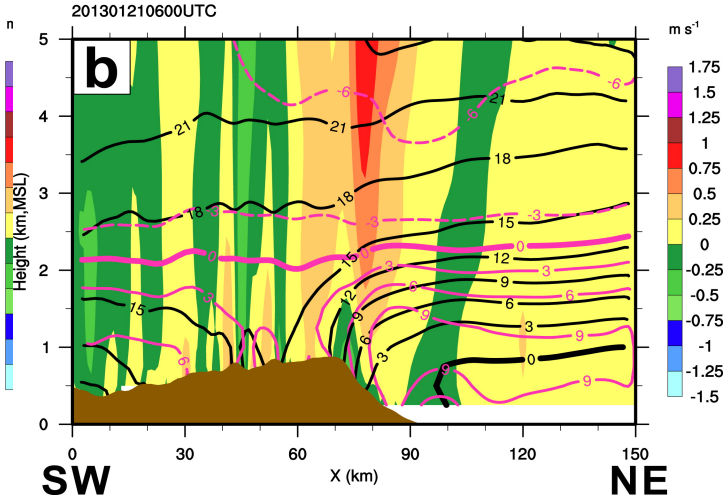

Fig 10 / 11

(a) shading: max reflectivity / Wind: cross barrier + 4*vertical velocity
(b) Shading: vertical velocity
Black contour: cross barrier flow (positive A/SW→A′/NE)
Purple contour: along barrier flow (positive: into the screen)

Structural evolution: Stage 2

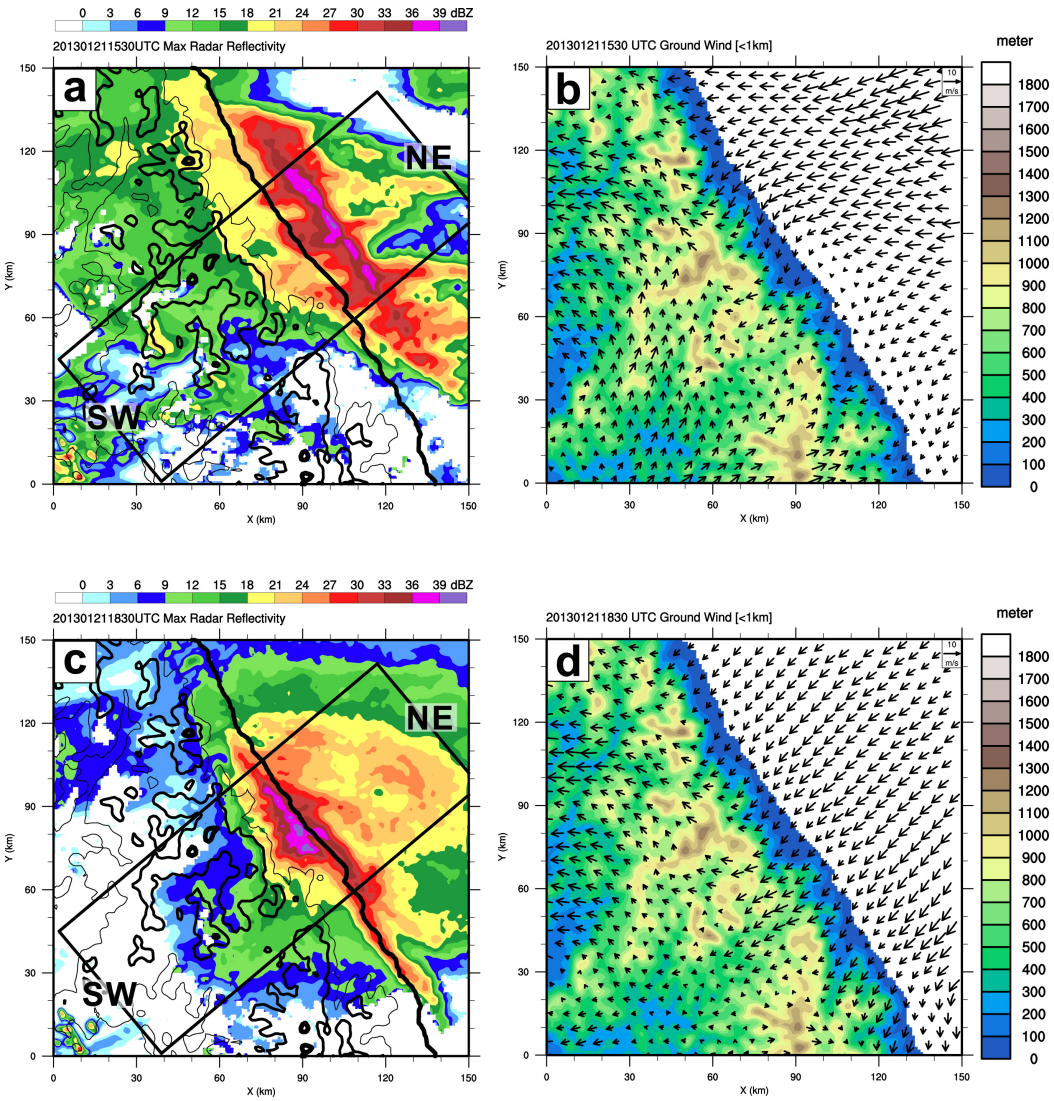

Fig 12 (ab) 1/21 1530 UTC (cd) 1830 UTC

(a) (c) shading: max reflectivity / Black contour: topography

(b) (d) Shading: topography / Wind: averaged ground-relative wind from WISSDOM (<1km MSL)

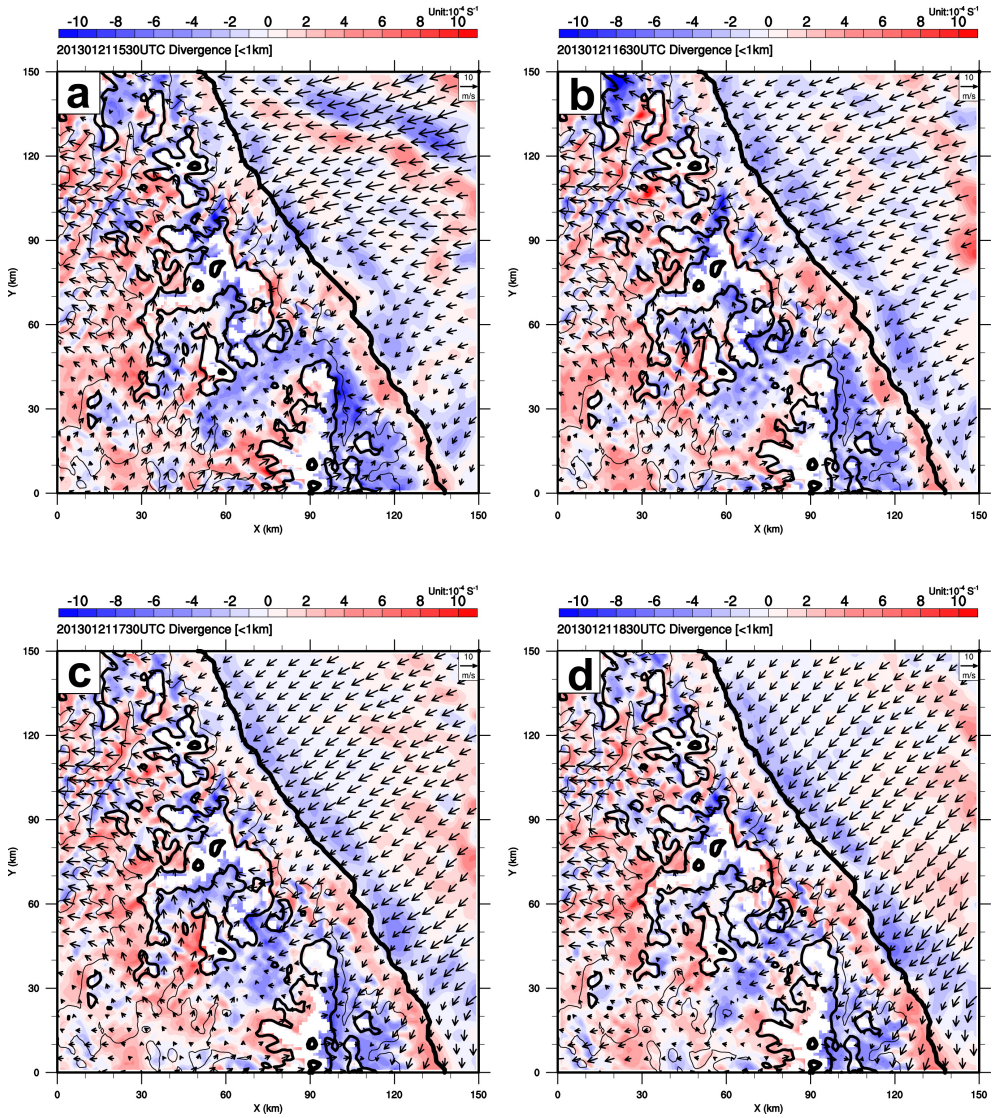

Fig 13 1530-1830 UTC Shading: Horizontal divergence (10^{-4}/s) / Black contour: topography

Structural evolution: Stage 2

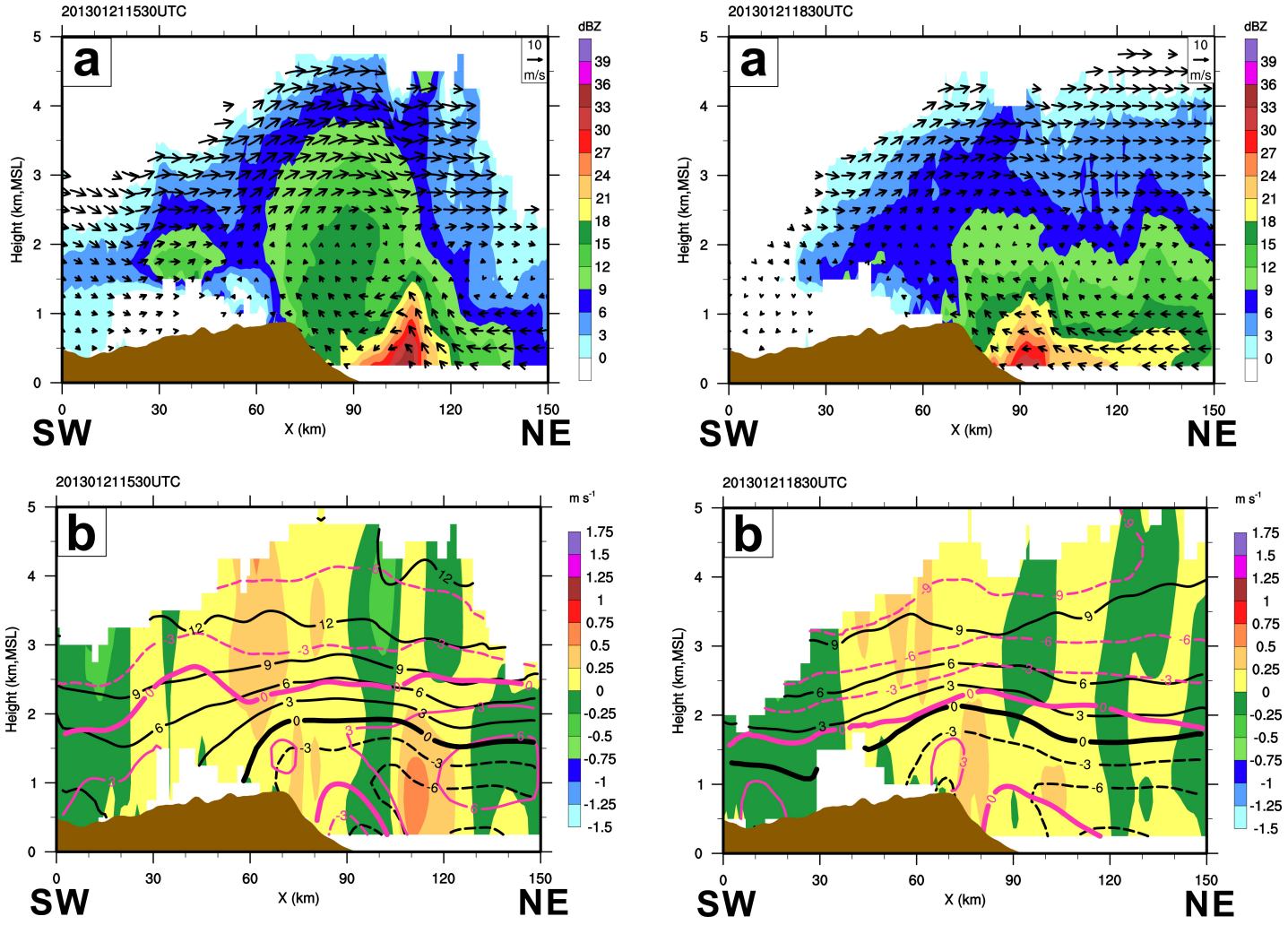

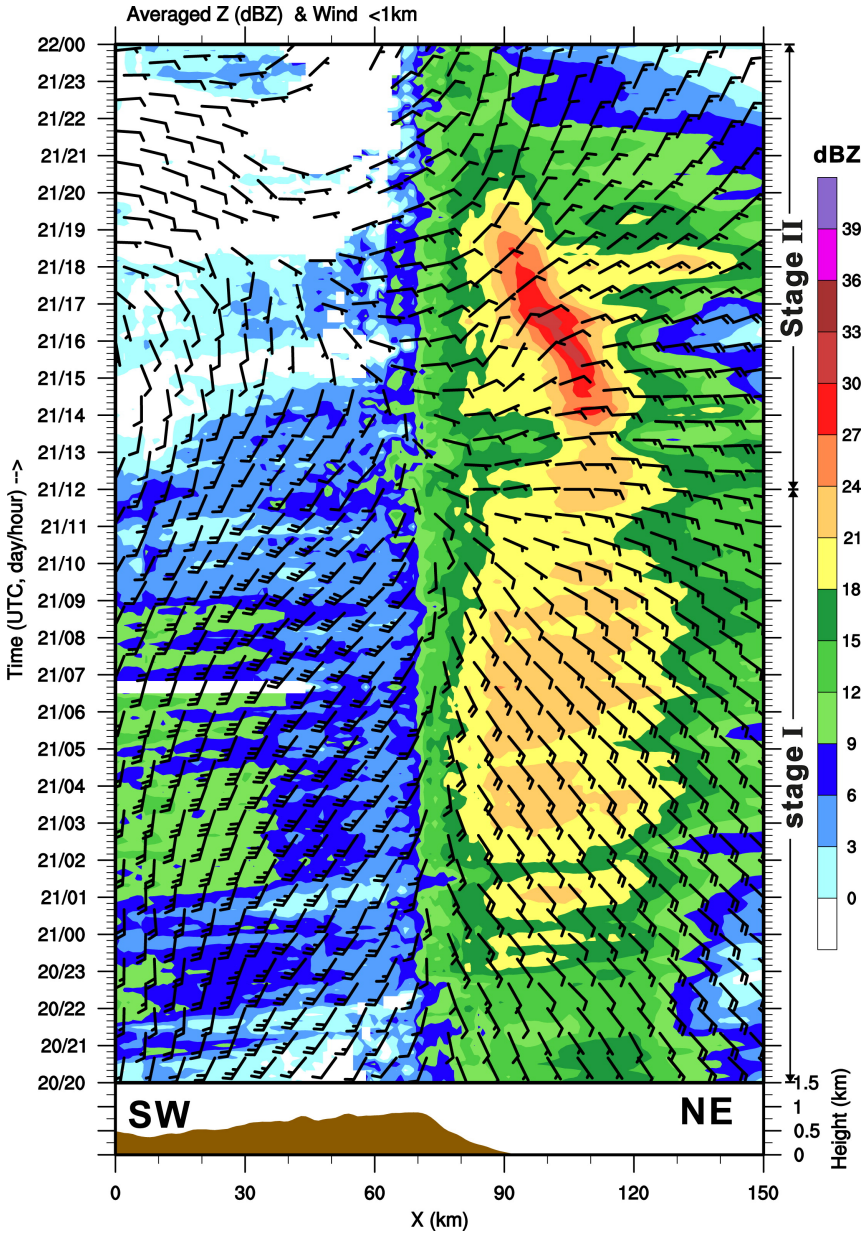

Fig 14 / 15 (a) shading: max reflectivity / Wind: cross barrier + 4*vertical velocity
(b) Shading: vertical velocity
Black contour: cross barrier flow (positive A/SW→A'/NE)
Purple contour: along barrier flow (positive: into the screen)

Conclusions

- Stage 1 (20Z 20 JAN – 12Z 21 JAN)
  - ➢ Wide spread precipitation:
    - circulation of LPS
  - ➢ Warm convection:
    - Prevailing winds exhibited veering changes from southeasterly to southwesterly with the height.
  - ➢ Precipitation (SW/ mid-level / downstream)
    - PCB-SW: The southwesterlies lifted over the terrain at the southwestern end of the PCB.
    - A zone of heavier precipitation associated with prevailing southwesterly winds, extending from the southwestern end to the northeastern side of the PCB.
    - downstream of PCB: mountain wave inducing upward motion, drifted precipitation particles, low-level convergence zone near the coast

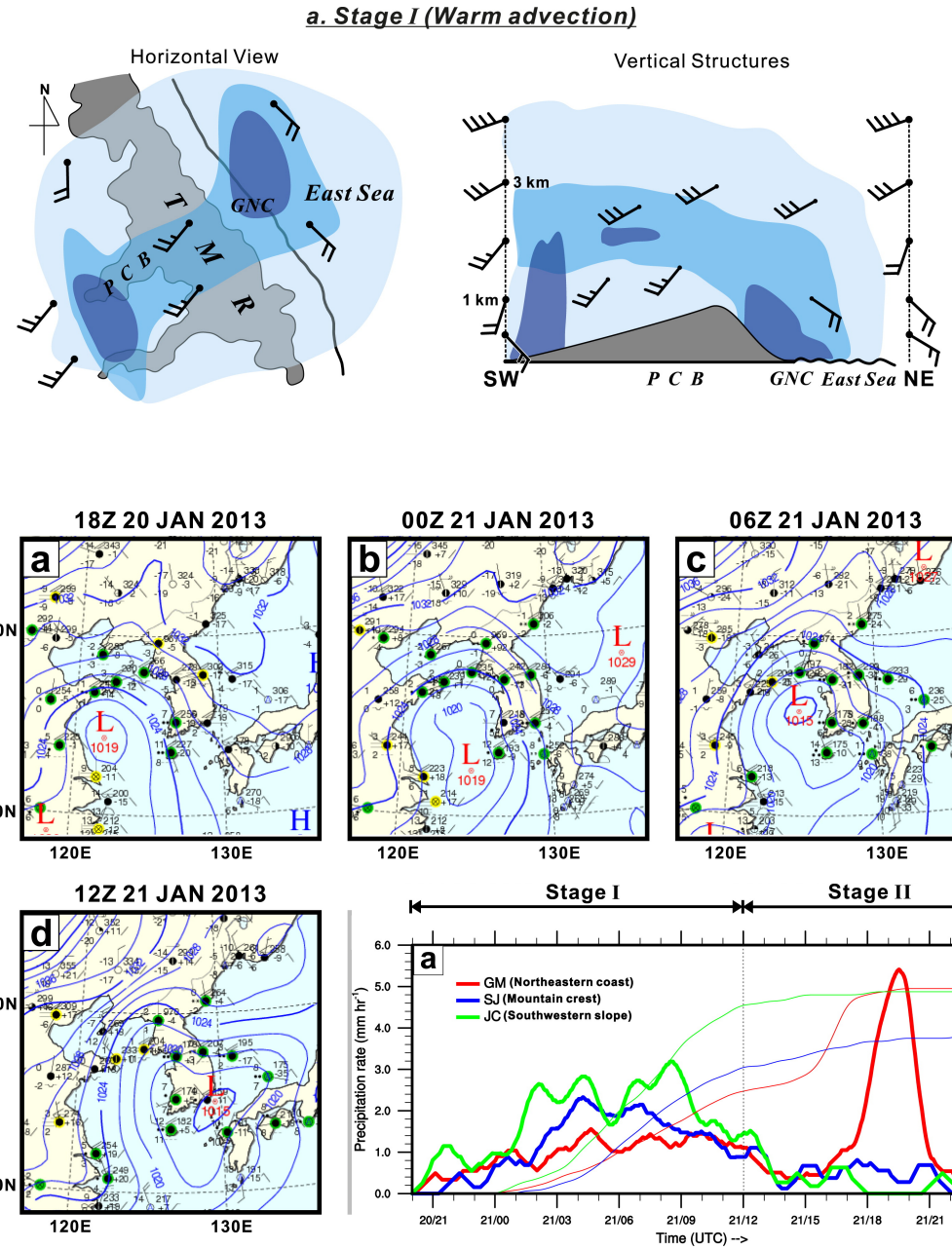

Conclusions

Stage 2 (20Z 20 JAN – 12Z 21 JAN)

- Change of the prevailing wind
  - more easterly, decelerated, turned parallel to the axis of the TMR, and developed a blocked zone along the coast.
- Convergence band
  - low-level oncoming flow encountered the nearshore blocked zone.
- When winds became northeasterly…
  - push the precipitation band inland
- Interaction of temporally changing winds accompanying the movement of an LPS over complex topography is a critical factor in determining the distribution and intensity of precipitation in the Pyeongchang area.

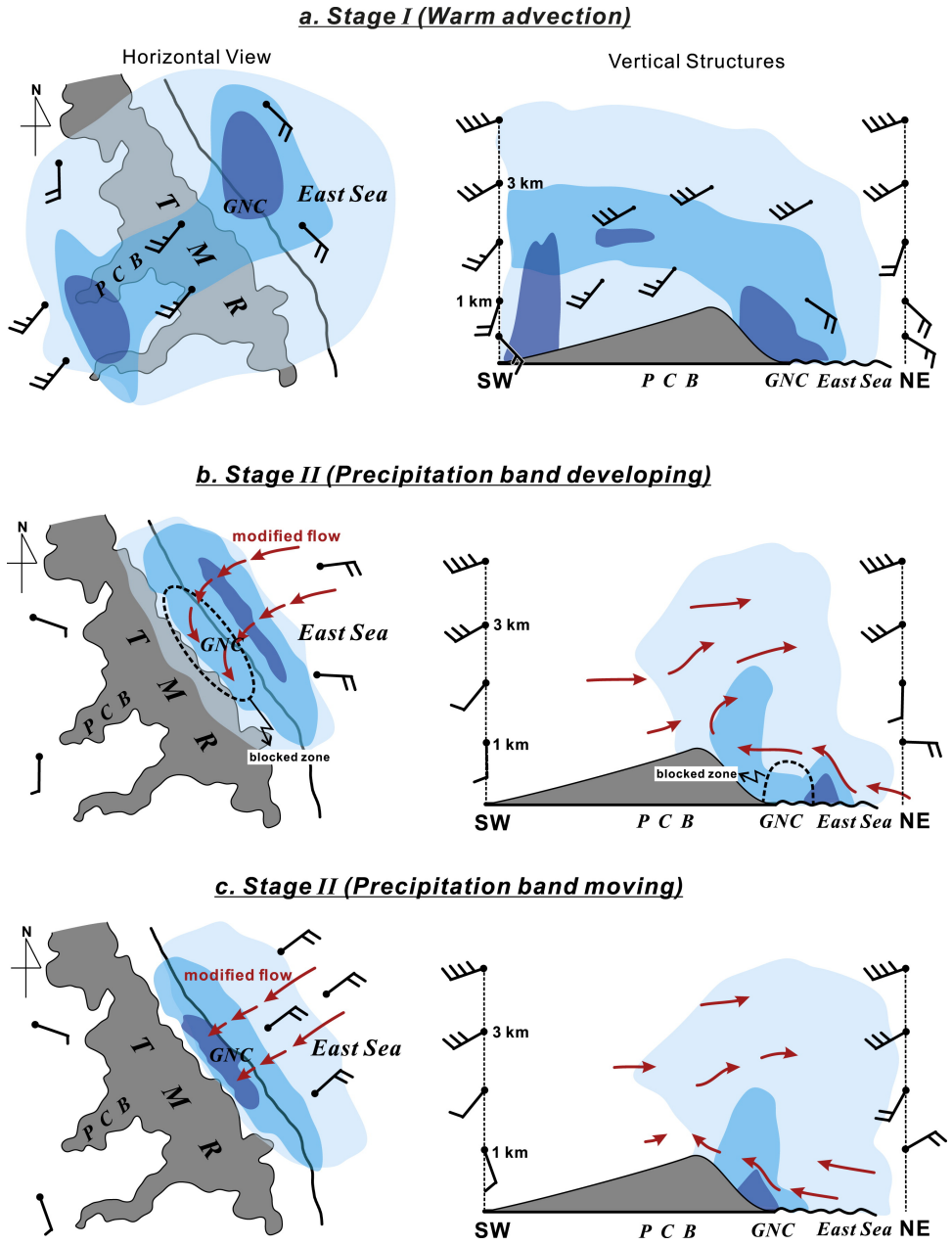

Characteristics of adopted radars

Parameters	GDK	GNG	WNJ	JWN	KAN	SBS
Longitude (°E)	127.43	128.86	127.96	127.89	128.94	128.44
Latitude (°N)	38.11	37.81	37.43	37.03	37.75	36.92
Radar height (m)	1064	99	120	117	27	1408
Wavelength (cm)	10.4	10.5	5.6	5.3	5.3	10.5
Beamwidth (°)	1	0.9	1	1	1	1
PRF (Hz)	599	535	1180	1200	1200	999
Nyquist velocity ($m\,s^{-1}$)	30.9	56.2	16.6	48.2	48.2	26.2
Max range (km)	250	280.25	89	125	125	149.12
Pulse width (μs)	1	1	1	0.8	0.8	1
Range resolution (m)	250	250	1000	1000	1000	125
Elevations (°)	0.0, 0.1, 0.2, 0.3, 0.6, 1.0, 1.7, 2.8, 4.6, 7.6, 12.3, 20	0.4, 0.6, 0.8, 1.1, 1.4, 1.8, 2.4, 3.0, 3.9, 4.9, 6.2, 7.9, 10, 12.7, 16, 20	1.6, 2.1, 2.8, 3.7, 4.9, 6.4, 8.3, 10.7, 13.7, 17.5, 22.2, 27.8, 34.4	1.8, 2.3, 2.9, 3.7, 4.6, 5.7, 7.1, 8.8, 10.8, 13.3, 16.3, 19.9, 24.2, 29.1, 34.6, 80	0.5, 0.9, 1.3, 1.8, 2.5, 3.3, 4.5, 5.9, 7.7, 10.1, 13.2, 17.1, 22, 28, 80	−0.5, 0.0, 0.3, 0.7, 1.0, 1.3

Zoom In